Electrochemical Characterization of the Open-Circuit Deposition of Platinum on Silicon from Fluoride Solutions

Pau Gorostiza,[†,‡,§] Philippe Allongue,[†] Raül Díaz,[‡] Joan Ramon Morante,[#] and Fausto Sanz*[,‡]

UPR 15 du CNRS, conventionné avec l'Université Paris 6, 4 Place Jussieu, Tour 22, Paris 75005, France, and Departament de Química Física and Departament d'Electrònica, Universitat de Barcelona, Martí i Franquès 1, Barcelona 08028, Spain

Received: January 17, 2003

An electrochemical study of the open-circuit deposition of platinum on silicon from fluoride solutions is presented. The main features of the process can be explained using the mixed potential theory, in which the electrode potential is defined by two simultaneous reactions at the electrode surface: a cathodic reaction (platinum reduction and deposition) and an anodic reaction (silicon oxidation and dissolution). The charge is exchanged through the semiconducting substrate. After an energy diagram for the cathodic and anodic sites has been developed, further details of the overall reaction are investigated; a simultaneous process of hydrogen incorporation into the silicon substrate is detected. This parallel reaction is the result of silicon etching at the anodic sites and is possibly enhanced by the presence of the metal on the surface. The electronic properties of the resulting interphase are discussed, together with the implications of these findings for the distribution of Pt nuclei during the deposition process. The results presented indicate that the coupling between the anodic and cathodic half-cell reactions is wider than a simple charge balance through the substrate.

1. Introduction

The open-circuit deposition of metals on silicon from fluoride solutions[1] has raised considerable interest recently, because of a great number of applications reported, including the delineation of junctions,[2] the revealing of crystallographic defects in wafers,[3,4] the investigation of the effect of trace metallic contaminants in silicon cleaning solutions,[5] the design of contamination sensors,[6,7] or the growth of photoluminescent porous silicon (PS) layers during metal deposition.[8] Metal electrodeposition from fluoride solutions has also been employed to fabricate high-quality Schottky diodes.[9] As more experimental data become available, the tendency is to investigate the mechanisms of deposition.[5,10−12] In the case of platinum, previous studies have shown that the process is electrochemical in nature and can be described using the mixed potential theory.[8,13,14] The reduction of Pt ions and the oxidation of Si atoms occur simultaneously at the silicon surface, in the absence of externally applied potentials (open-circuit potential, OCP). Fluoride is a complexing agent of silicon that dissolves the oxide at the surface. The working principle is thus similar to the "electroless" or displacement deposition of a metal onto a less-noble substrate. However, several aspects remain unclear, such as the morphologic distribution of metal nuclei over the surface, the differences between the behavior of *n*- and *p*-type electrodes, or the absence of hydrogen evolution during the silicon etching reaction. These effects are not explained directly by the mixed potential theory and require a more-detailed study.

Here, we present a complete electrochemical characterization of the OCP deposition of platinum on silicon. The aim is to sketch, as detailed as possible, an energy diagram for the interface between silicon and an aqueous fluoride solution containing Pt(II) ions to discuss the electrochemical processes at the interface. This allows us to discuss, in detail, issues such as the presence of parallel, coupled reactions, the electronic properties of the resulting surface region, or the distribution of deposited nuclei over the electrode surface, which were poorly understood.

2. Experimental Section

The silicon substrates employed in this study were manufactured by Siltronix; the substrates were (100)-oriented and occasionally (111)-oriented, both *n*-type (P-doped, 1 Ω cm resistivity, $N_D \approx 5 \times 10^{15}$ cm^{-3}) and *p*-type (B-doped, 1 Ω cm resistivity, $N_A \approx 10^{16}$ cm^{-3}), and polished on one side. At these doping densities, the Fermi energy is located at $\mu_C \approx 0.25$ eV below the conduction band (CB) in *n*-type silicon and at $\mu_V \approx 0.2$ eV above the valence band (VB) in *p*-type silicon.[15] To make an ohmic contact, the back of the sample was painted with InGa alloy at the eutectic point and then contacted to a metallic plate. Prior to measurements, samples were first electropolished so that the experiment could begin with a substrate that was free of eventual H-related subsurface defects. The electropolishing procedure has been described elsewhere.[12,16] Prior to the experiments, the remaining oxide was dissolved in HF (40%) for a few seconds, until the surface showed a hydrophobic behavior (H-terminated).

All electrochemical experiments were conducted in darkness, and only the polished side of the silicon samples was exposed to the solution, through a window in the cell (with an area of 0.3 cm^2). An HQ Instruments model 105 potentiostat was used with a saturated calomel electrode (SCE) as the reference and a platinum grid was used as the counter electrode. Solutions were prepared with MilliQ water. The HF concentration was 2 M to obtain pH 2. In certain cases, 0.6 M NH_4F solutions at

* Author to whom correspondence should be addressed. E-mail: f.sanz@qf.ub.es.
† UPR 15 du CNRS.
‡ Departament de Química Física, Universitat de Barcelona.
§ Present address: Departments of Physics and Molecular and Cell Biology, University of California at Berkeley, Berkeley, CA.
# Departament d'Electrònica, Universitat de Barcelona.

10.1021/jp030071v CCC: $25.00
Published on Web 06/07/2003

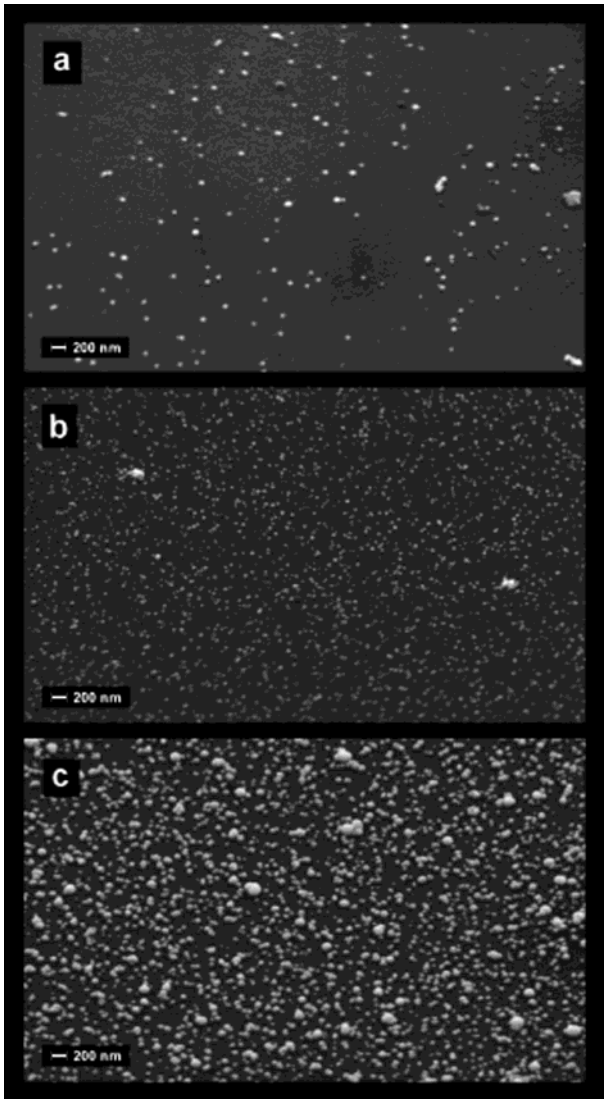

Figure 1. SEM images of a *p*-type silicon sample after deposition under an injection current of 150 μA/cm^2 in 2 M HF, 200 μM $PtCl_4^{2-}$ solution for (a) 10, (b) 20, and (c) 50 s. The progressive nucleation of Pt nuclei can be appreciated. The corresponding atomic concentrations, measured by RBS, are 0.11×10^{15}, 6.7×10^{15}, and 33×10^{15} atoms/cm^2.

pH 4.5 were used. Divalent platinum was added as K_2PtCl_4 salt (Johnson−Matthey) with a concentration in the range of 30 μM to 2.5 mM. Impedance measurements were performed with a Solartron model 1174 frequency response analyzer, using a measurement signal of 10 mV at 25 kHz. A classical resistor−capacitor parallel equivalent circuit was assumed in calculating the capacitance. Flatband (FB) potentials were determined by extrapolating the plotted $1/C^2$ vs U curves at $1/C^2 = 0$, using the Mott−Schottky (MS) relationship, where C is the space-charge layer capacitance of the semiconductor and U is the applied potential.

Platinum deposits were characterized via scanning electron microscopy (SEM) and electron-dispersive X-ray spectroscopy (EDX), using Leica model Stereoscan S-360 and Cambridge model S-120 (equipped with a Link model AN-10000 EDX apparatus) equipment. Atomic force microscopy (AFM) was performed with a Multimode Nanoscope IIIa operated in tapping mode. Rutherford backscattering spectroscopy (RBS) measurements were performed with the 2 MeV Van de Graaff accelerator at the Groupe de Physique des Solides (Université Paris 7) to dose the surface density of Pt atoms after deposition.

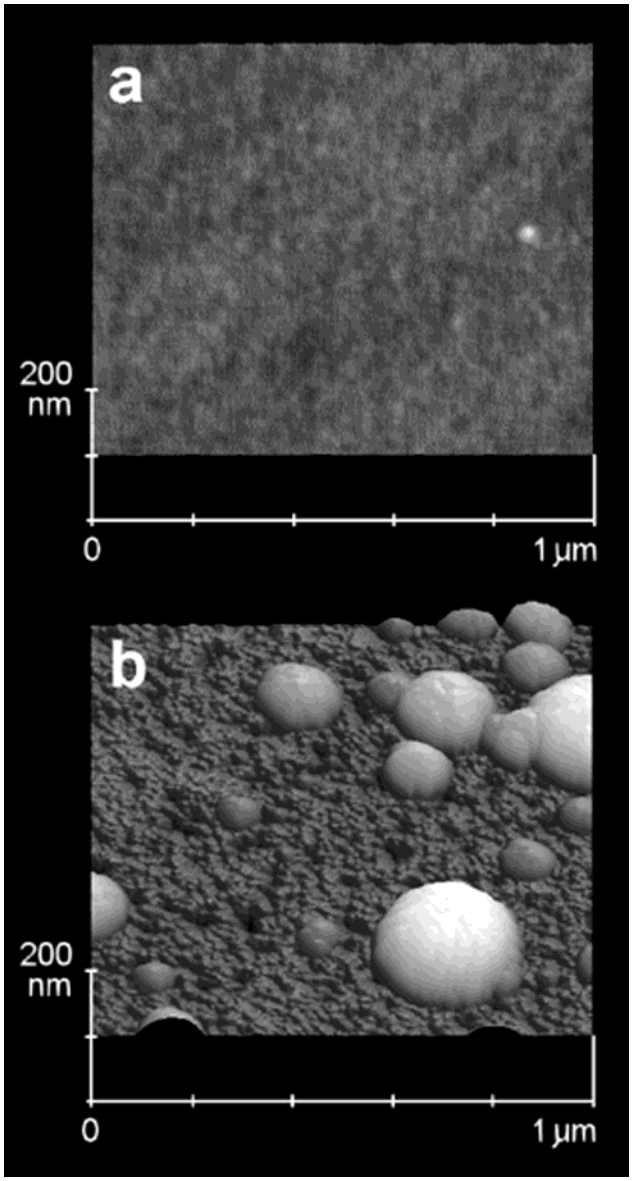

Figure 2. Tapping-mode AFM images of a *p*-type silicon sample (a) before and (b) after 10 min of deposition of platinum from a 2 M HF, 200 μM $PtCl_4^{2-}$ solution. The topography of the Pt nuclei and the increase in the roughness of the silicon can be appreciated. Only the polished side of the silicon was exposed to the deposition solution.

3. Results

3.1. Microscopy Observations. After few minutes of immersion in the fluoride solution containing Pt(II) ions, a layer can be observed to the naked eye. A detailed inspection using SEM revealed the presence of bright nuclei a few hundred nanometers in size, and EDX measurements confirmed that these nuclei are composed of platinum. Figure 1 shows samples after deposition for 10, 20, and 50 s under an injection current of 150 μA/cm^2. The corresponding atomic concentrations measured by RBS are 0.11×10^{15}, 6.7×10^{15}, and 33×10^{15} atoms/cm^2. AFM imaging (Figure 2b) shows quite large metallic nuclei on the silicon surface. Etch pits are between the nuclei, and a general increase in substrate roughness is observed, with respect to the original surface (Figure 2a). Observations were very similar with both *n*- and *p*-type silicon samples. The main differences concerned the distribution of nuclei and etch pits over the surface.[13,14] The *p*-type samples display a uniform etching on the surface with platinum deposition occurring with

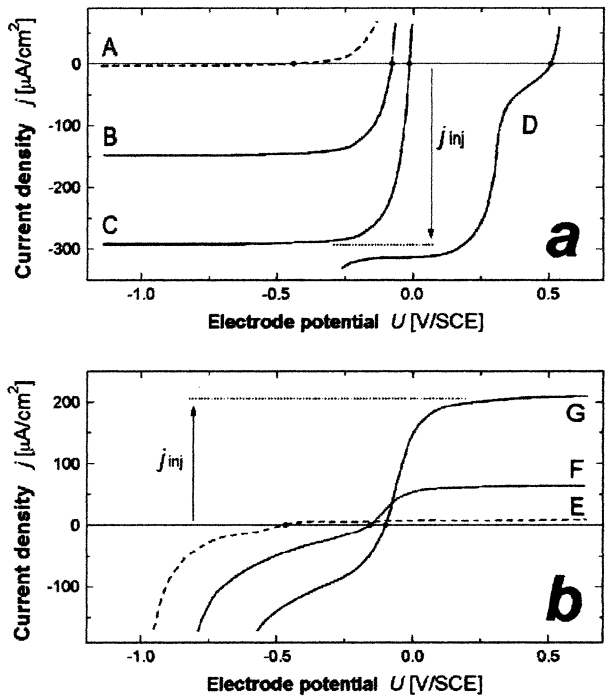

Figure 3. (a) Dark current−potential curves of a *p*-type silicon electrode (curves A, B, and C) and a platinum electrode (curve D) immersed in a 2 M fluoride solution. Curve A corresponds to the blank solution (no metal added), curve B corresponds to 300 μM $PtCl_4^{2-}$, and curves C and D correspond to 2.5 mM $PtCl_4^{2-}$. (b) Dark current−potential curves of an *n*-type silicon electrode immersed in a 2 M fluoride solution (curve E) and after the addition of 300 μM $PtCl_4^{2-}$ (curve F) and 2.5 mM $PtCl_4^{2-}$ (curve G).

a progressive nucleation process. On *n*-type substrates, the process has a more local character, because platinum nuclei and deep etch pits are found very close to each other; in some instances, platinum nucleates at the bottom of the etch pits or pores, and nuclei grow at the expense of the surrounding silicon, forming a buried layer.[14]

3.2. Electrochemical Characterizations. The system was characterized by measuring the $j-U$ curves in darkness and in the absence of stirring. They are shown in Figure 3a (*p*-type) and b (*n*-type), where the dashed lines (A in Figure 3a, E in Figure 3b) correspond to the supporting fluoride solution and the solid lines (B−D in Figure 3a, F−G in Figure 3b) correspond to different Pt(II) fluoride solutions. An increase in the reverse current in *p*-type silicon (cathodic) occurs in the presence of $PtCl_4^{2-}$ ions, and this current is proportional to the Pt(II) concentration in solution. For *n*-type silicon, the anodic branch of the current varies linearly with the Pt(II) concentration. In the 2.5 mM Pt(II) solution, the $j-U$ curve of the platinum electrode (curve D) displays a cathodic plateau with an amplitude close to that found with *p*-type silicon in the same solution. The intensity of the plateaus is plotted in Figure 4, as a function of the Pt(II) concentration. The log−log scale slope is ∼1.0 for *p*-type silicon and only 0.4 for *n*-type silicon. The same results were qualitatively obtained by recording the $j-U$ curves while stirring the Pt(II) solution, meaning that the reaction is limited by mass transport in solution.

3.3. Energy Diagram of the Interface. The electron energy diagram of the interface (Figure 5) was built from the Mott−Schottky (MS) plots and OCP values. U_{FB} and OCP values are collected in Table 1. The position of the CB and VB edges accounts for the energy difference between the Fermi level and the CB minimum ($\mu_C \approx 0.25$ eV) or the VB maximum ($\mu_V \approx 0.20$ eV). Dashed lines refer to the situation in the blank fluoride solution and the solid lines correspond to the Pt(II)-containing solution. In the electrolyte, the redox level of the system $PtCl_4^{2-}$/Pt is $E°(PtCl_4^{2-}/Pt) = +0.3$ V/SCE. The system H^+/H_2 is located at $E°(H^+/H_2) = -0.3$ V/SCE.

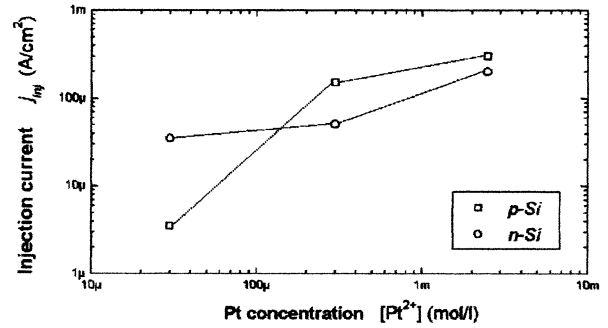

Figure 4. Hole-injection currents (j_{inj}) at different $PtCl_4^{2-}$ concentrations in the common electrolyte (2 M fluoride). Current values are obtained from the cathodic and anodic plateaus of Figure 3a (*p*-type silicon) and b (*n*-type silicon), respectively.

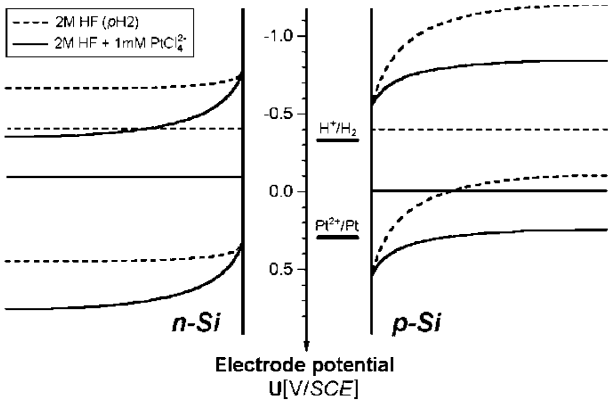

Figure 5. Experimental energy diagram of the interface between silicon and a fluoride blank solution (- - -) at pH 2 and (—) in the presence of 1 mM Pt^{2+}/Pt. Steady-state conditions are readily achieved in a few minutes, because of the high Pt(II) concentrations employed.

TABLE 1: Parameters Used to Determine the Energy Diagram of the Interface at the Rest Potential

	blank solution			platinum solution[a]		
	U_{FB}/V	OCP/V	V_B/V[b]	U_{FB}/V	OCP/V	V_B/V[b]
n-type Si	−0.5	−0.4	+0.1	−0.5	−0.1	+0.4
p-type Si	+0.4	−0.4	−0.8	+0.4	∼0	−0.4
n-type Si/Pt	−0.1			−0.1	+0.4	+0.5

[a] The given values were only slightly dependent on the Pt(II) concentration of the solution, which was between 30 μM and 2.5 mM, whose Nernst potential is $E° = 0.37$ to $+0.42$ V. [b] $V_B = OCP - U_{FB}$, the value of which is >0 for *n*-type Si (downward bending) and <0 for *p*-type Si (upward bending).

It is important to recall that the interface is essentially heterogeneous in the Pt(II) solution. The aforementioned energy diagram is *averaged* over the entire interface. To determine the energy diagram *at the metal nuclei*, an *n*-type silicon sample was covered with a *continuous* platinum film, so that the electrolyte does not contact the silicon surface. This limiting case is known as the "Schottky electrode".[17] We assume that, locally, the energy diagram at the Si/Pt nucleus will be close to that of the continuous layer. The platinum layers were grown from 0.1 M H_2SO_4 + 1 mM $PtCl_4^{2-}$ solutions at a potential between −1.5 and −2.0 V/SCE ($j \approx -10$ mA/cm²) for 10 min. As anticipated, the OCP value of the *n*-type Si/Pt Schottky electrode is similar to the Nernst potential of the platinum solution, because all Fermi levels are aligned at equilibrium

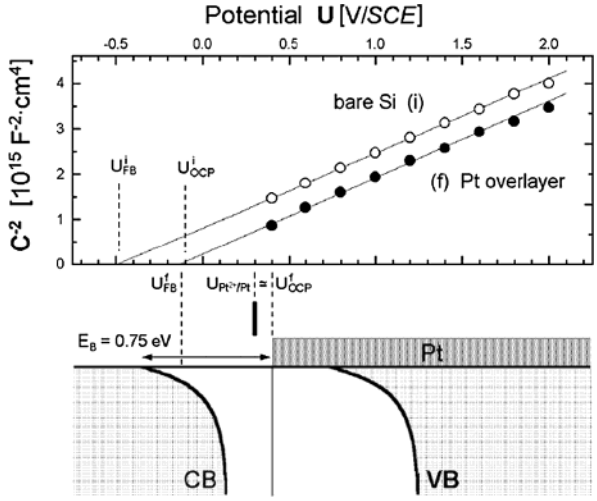

Figure 6. (a) Mott−Schottky (MS) plots of (○) bare silicon and (●) a Pt/*n*-type Si Schottky electrode in a Pt(II) solution.

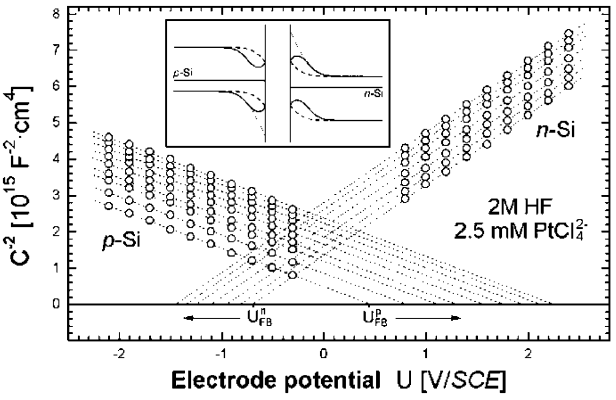

Figure 7. Time evolution of MS plots in *n*- and *p*-type silicon exposed to a 2 M HF, 2.5 mM $PtCl_4^{2-}$ solution at the open-circuit potential (OCP). Inset shows that the flatband (FB) potential is given by the initial extrapolation (dashed lines). The shift of the subsequent plots is interpreted as indicated by the dotted lines (see text for details).

(Figure 6). The metallic surface is in equilibrium with both the *n*-type silicon and the solution. Given the U_{FB} value, the corresponding barrier height of the Schottky contact between *n*-type silicon and platinum is $\phi_B = V_B + \mu_C = +0.75$ V, which is the expected value for such a contact.

3.4. Time Evolution of U_{FB} in the Platinum Solutions. The values given in Table 1 were recorded immediately after immersion in the Pt(II) solution. The FB potential was observed to shift with the deposition time. The time evolution of the MS plots of *n*- and *p*-type silicon in a 2 M HF + 2.5 mM $PtCl_4^{2-}$ solution is shown in Figure 7. The time given in the figure refers to the time of immersion at OCP. The initial value $U_{FB}°$ was obtained from the MS plot in the "blank" fluoride solution. After addition of the Pt(II) salt, the sample was kept at OCP and capacitance plots were subsequently acquired every 5 min. The series shown in Figure 7 indicates that the FB shifts by almost +1.7 V within 1 h for a *p*-type silicon electrode; the shift is negative and only −0.5 V for *n*-type silicon. The results of Figure 7 have been replotted in Figure 8 as the square root of ΔU_{FB} versus the square root of time *t* for different platinum concentrations. This representation will be used to fit the parabolic variations expected from the model given in the Appendix.[16] For the sake of convenience, the experimental data for *n*-type silicon have been plotted as the negative square root of ΔU_{FB}, as a reminder that the shift is negative. The Pt(II) concentration is indicated.

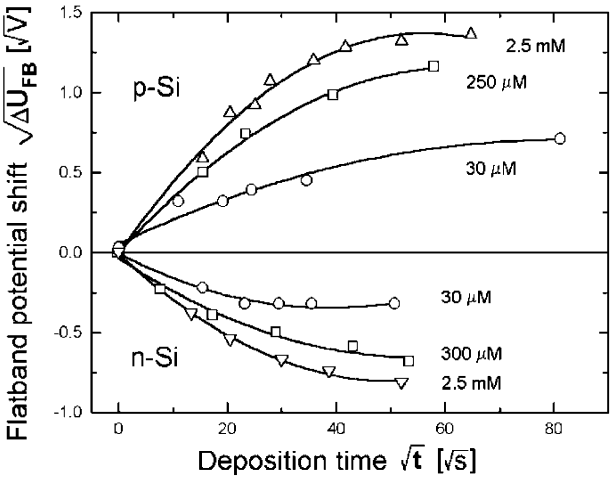

Figure 8. Parabolic fit of the FB potential shifts obtained from Figure 7 at the OCP, and different $PtCl_4^{2-}$ concentrations. Values of $\sqrt{\Delta U_{FB}}$ for *n*-type silicon have been plotted as negative, as a reminder that MS plots shift toward negative potentials. The abscissa corresponds to the deposition (and etching) time at the OCP. Each experimental point in the series is the extrapolation of one MS plot, relative to its initial value (freshly electropolished silicon in HF alone).

To check whether the aforementioned phenomenon is related to the formation of the platinum phase or to the associated dissolution, the same experiment was conducted with *p*-type silicon samples immersed at −2 V/SCE (where no electrochemical dissolution occurs) instead of OCP. In the $PtCl_4^{2-}$ solutions whose concentrations were between 30 μM and 2.5 mM, MS plots remained *unchanged* under these conditions. Even after immersion for 1 h, the extrapolation always gave the "initial" $U_{FB}°$ value that was found in the platinum-free fluoride solution. Finally, Figure 9 compares the shift of MS plots of *p*-type Si(111) samples (1 Ω·cm) during platinum deposition at the OCP ($j_{inj} = 125$ μA/cm²) and during anodization (110 μA/cm²), both in a fluoride solution of pH 4.5. As discussed below, the similarity of curves suggests that the displacement of the FB is related to hydrogen diffusion into silicon.[16]

4. Discussion

4.1. Electrochemical Reactions at the Silicon/Solution Interface at the Open-Circuit Potential. *4.1.1. Blank Solution.* In the absence of metal ions, the Fermi level of *n*- and *p*-type silicon electrodes lies close to $E(H^+/H_2)$ at the OCP. This steady-state equilibrium can be described as a dynamic equilibrium between two opposite reactions: the anodic one being the dissolution of the substrate and the other being the reduction of protons (H_2 evolution) and dissolved oxygen.[1,18−20] The small band bending in *n*-type silicon (Table 1) means a great density of CB electrons at the surface and, therefore, suggests a slow kinetics for the cathodic reaction, because the rate of silicon dissolution is very small at such low pH.[21] The etching rate of silicon is indeed <1 Å/min at pH 2. This corresponds to an exchange current of <2.6 μA/cm². This very small anodic current explains that the band bending is maximum in *p*-type silicon. In this case, any decrease of the band bending would lead to an anodic current (associated with the thermionic emission of holes over the surface barrier) much larger than 2.6 μA/cm². The smallest possible cathodic current corresponds to carrier recombination in the space-charge layer.[22]

4.1.2. Pt(II) Solution. After the addition of $PtCl_4^{2-}$, the Nernst potential of the solution lies now close to the VB of silicon at

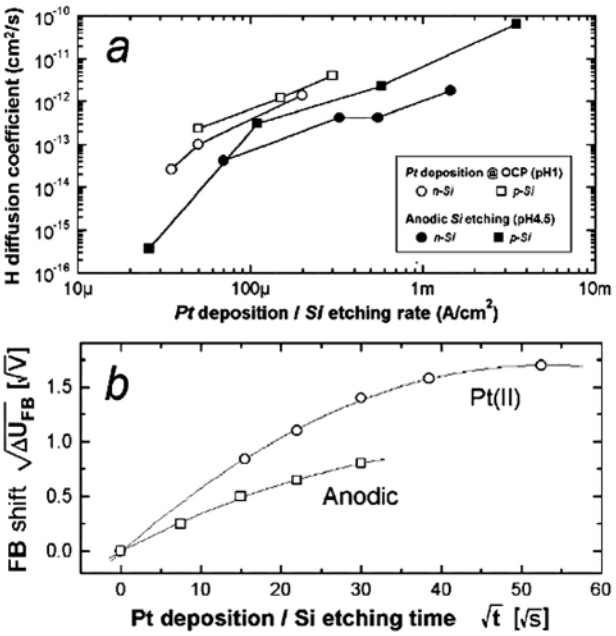

Figure 9. (a) Apparent diffusion coefficients of hydrogen in silicon (D_H), as a function of the etching rate. Figure 9a also shows a comparison between platinum deposition experiments at the OCP (open symbols; silicon etch rate estimated from j_{inj} measurements at reverse bias) and anodic etching experiments (filled symbols; etch rate calculated from the anodic current, using data from ref 32). (b) Shift of the MS extrapolation versus silicon etching time. Solution pH and silicon etching rate were fixed, and the comparison was made between platinum deposition at the OCP and anodic etching experiments. D_H value obtained is larger for the platinum deposition process (see text).

the surface (Figure 5). The *injection of holes* into the semiconductor VB becomes, therefore, possible.[21] The presence of Pt(II) ions sets a hole injection current that is proportional to the overlap between the empty states in solution and occupied states in the solid. This current is, hence, independent of the applied potential within the plateau, because the density of occupied states in silicon is constant and much greater than that of empty states in solution. The injection current is equal to the cathodic plateau of the $j-U$ curves of *p*-type silicon electrodes, because, in that case, all injected holes are swept away from the surface region and collected at the rear ohmic contact, because of the favorable band bending. A verification is provided by the fact that the current plateaus at *p*-type silicon and platinum electrodes are equal under cathodic bias. With *n*-type silicon electrodes, the cathodic plateau should be also observed. It is less well marked, because the accumulation of electrons at the surface promotes the reduction of protons. To a first approximation, we will assume that holes are injected at the same rate into *n*- and *p*-type silicon.

At the OCP, the corrosion rate is $j_{corr} = -j_{inj}$. Consistently, the downward band bending in *n*-type silicon keeps the injected holes close to the surface, which promotes dissolution after their capture in Si−Si surface bonds. The effect is associated with the anodic current measured in darkness (see below). In the case of *p*-type silicon, the effect manifests itself by a decrease of the band bending (Table 1), which promotes thermionic emission of holes over the barrier. This leads also to dissolution. In the conditions of our experiments, j_{inj} is controlled by mass transport in solution, because it depends on the $[PtCl_4^{2-}]$ concentration and solution stirring. The magnitude of the corresponding dissolution current ($j_{corr} = -j_{inj}$) remains much smaller than the current threshold (~20 mA/cm²) necessary to enter the electropolishing regime of silicon in 2 M HF solution.[8] Thus, the anodic dissolution is expected to lead to the formation of a porous silicon (PS) layer. The enhanced roughness in Figure 2B may be attributed to the PS layer between Pt clusters. The AFM image illustrates the spatial separation of the anodic and cathodic sites coexisting on the surface at the OCP.

At anodic bias and for *n*-type silicon, the holes are injected at the same rate as that at the OCP and promote anodic dissolution with the same rate. This explains the increase of the anodic current in Pt(II) solutions, with respect to the blank one. This anodic current, measured in darkness, is related the injection of electrons. It is well-known that the anodic dissolution of *n*-type silicon may be described by the simplified reaction[21,23,24] $h^+ + Si \rightarrow Si(II) + e^-_{CB}$, which expresses that an electron is produced at the surface and injected into the CB from some activated energy level at the surface. More details are given in Gerischer's original paper.[25] This electron is collected at the rear ohmic contact, because of the downward band bending in *n*-type silicon. The amplitude of the anodic current should be equal to $-j_{inj}/2$. Experimentally, it is nevertheless smaller than expected from the previously given equation. A tentative explanation is given in the next paragraph. The process probably also occurs in *p*-type silicon but is masked by the exponential growth of the current.

4.1.3. Comparison of the Structure of Naked Silicon with Anodic Porous Silicon Formation. As discussed previously, the dissolution accompanying the deposition should lead to PS formation. The roughness of the substrate (Figure 1b) is consistent with a certain porosity. In addition, visible photoluminescence (PL), which is another well-known property of anodized PS,[26] is also found with our samples after OCP deposition of platinum from fluoride solutions. Under UV light, samples display an orange-red glow that is visible to the naked eye.[8]

Despite the strong similarity between the PS layer formed during platinum deposition at the OCP or under anodic conditions, one feature is remarkably absent during the OCP deposition of platinum. Indeed, no hydrogen evolution is visible. The H_2 bubbles formed during silicon anodization (in the PS regime)[27,28] or during stain etching[29] are not observed in our case. This "anodic H_2 evolution", which results from the homogeneous (i.e., in the solution phase) hydrolysis of silicon etch products[20] according to the schematic reaction $Si(II)_{sol} + H_2O \rightarrow Si(IV)_{sol} + H_2\uparrow$, should be observed, because PS is formed. The last chemical reaction is purely schematic, and the details have been omitted; it is meant to outline the reaction products formed close to the surface of the electrode. The difference between our situation and standard anodization is the presence of Pt nuclei. We infer that the H_2 is reoxidized according to the reaction $H_2 \rightarrow 2H^+ + 2e^-$. The position of the Fermi level of the Pt nuclei, close to +0.4 V (Figure 6 and Table 1), is indeed more positive than the standard potential $E°(H/H^+)$. The produced electrons have an energy similar to that of the Fermi level of Pt clusters. They may either be reemitted from the Pt clusters into the silicon (thermionic emission) or recombine with holes. This last process is more likely, with the interface states at the Pt/Si contacts acting as recombination centers. This, in turn, would explain that the measured anodic current at *n*-type silicon (Figure 4) is smaller than expected.

In summary of this subsection, it has been shown that, when a silicon electrode is exposed to a fluoride solution containing $PtCl_4^{2-}$ ions, two reactions proceed simultaneously on the electrode surface at the OCP. First, Pt(II) ions are reduced to metallic platinum by injecting holes into the Si VB (cathodic

TABLE 2: Concentration of Pt(II) Ions ([Pt(II)]), Hole-Injection Current (j_{inj}), Diffusion Coefficient of H Species (D_H), Relative Surface Doping ($N_S/N_{A,D}$), and Depth of Subsurface Layer (δ) for *p*- and *n*-Type Silicon

Si	[Pt(II)]	j_{inj} (A/cm^2)	D_H (cm^2/s)	$N_S/N_{A,D}$	δ (nm)
p	30 μM	5×10^{-5}	2.3×10^{-13}	+0.28	192
p	300 μM	1.5×10^{-4}	1.2×10^{-12}	+0.25	320
p	2.5 mM	3×10^{-4}	4.0×10^{-12}	+0.60	540
n	30 μM	3.5×10^{-5}	2.6×10^{-14}	−16.5	30
n	300 μM	5×10^{-5}	1.0×10^{-13}	−5.5	85
n	2.5 mM	2×10^{-4}	1.4×10^{-12}	+0.05	290

half-cell reaction). Second, the capture of the injected holes at the electrode surface results in silicon oxidation and dissolution in the presence of a fluoride species (anodic half-cell reaction). The overall process is limited by diffusion of $PtCl_4^{2-}$ ions to the silicon surface. As free charge carriers, the injected holes can travel inside the semiconductor, so the cathodic and anodic reactions are spatially occurring from different regions of the surface (called *anodic* and *cathodic sites*).

Although the energy diagrams of Figure 5 help to illustrate the overall process, they must be refined to account for the heterogeneity of the surface. Growing metal nuclei are present at the cathodic sites, and a dissolution reaction is underway at the bare silicon regions (anodic sites). They are treated separately in the two next sections.

4.2. Hydrogen Permeation Induced by Platinum Deposition. The results in Figure 9b support the hypothesis that progressive hydrogen permeation occurs in the silicon electrode during the silicon dissolution reaction. This would be consistent with the fact that the deposition process is balanced by PS formation. It is known that PS formation leads to the incorporation of hydrogen into silicon.[16] The absence of any FB shift upon the immersion of *p*-type silicon electrodes at cathodic bias is further supporting the hypothesis that the shift of U_{FB} is associated with the counter reaction (dissolution reaction). By depositing platinum under a cathodic potential, holes are indeed swept away from the surface, which prevents any silicon dissolution.

The details of the mechanisms of hydrogen migration into silicon are rather complex. The mechanism depends on the doping level and the type of conduction of the substrate. In *p*-type silicon, the negatively charged dopants are complexed by H^+ cations and a perfect doping *compensation* is observed.[30,31] Its extension depends on time and potential (field-enhanced migration). This mechanism explains very well the parallel displacement of the MS plots, because the compensated layer acts as a dielectric capacitance in series with the space-charge capacitance. In *n*-type silicon, the situation is less simple. There is a decay of the concentration of H species. In this case, there is an overdoping under the surface. This also shifts the extrapolation of the MS relationship.

As can be seen in Figure 8, the fit of data is quite good, using the model described in the Appendix and originally built for anodized silicon.[16] Curve fitting was performed using the dissolution rate $R = -j_{inj}$. Table 2 lists the diffusion coefficient of H species (D_H), the relative surface doping ($N_S/N_{A,D}$; a negative sign indicates that the surface doping is opposite to bulk doping) and the depth of the subsurface layer (δ). The value of δ corresponds to the *final* situation, i.e., at the end of the experiment. The subsurface region appears to be slightly thinner in *n*-type silicon substrates and has *p*-type character at low corrosion rates. In *p*-type silicon, the subsurface layer is p^- (this is consistent with acceptor compensation). The mean value of D_H is approximately one order of magnitude larger during platinum deposition than during anodization experiments.

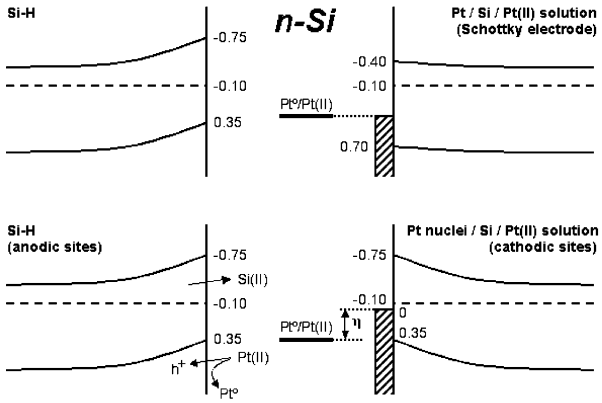

Figure 10. (Top) Theoretical band diagram for the bare and platinum-covered *n*-type silicon surface (see text for the construction). (Bottom) Modified band diagrams. Note the upward shift of the band edges on the cathodic sites. The anodic sites remain unchanged.

This effect may attributed to the fact that the proton concentration is enhanced close to the surface, because of the reoxidation of H_2 on Pt clusters (see previous discussion). This creates a "barrier" against proton diffusion toward the solution and enhances the probability of hydrogen incorporation into silicon.[32] This mechanism is clearly not possible in the absence of Pt nuclei (anodic silicon oxidation).

4.3. Energy Diagrams. The energy diagrams shown in Figure 5 (solid lines) give the *averaged* position of the band edges and band bending. We recall that the surface is heterogeneous, because it is composed of Pt clusters and naked PS silicon (Figure 2b). Knowing that we have anodic and cathodic sites on the surface, we may attempt to build a more complete band diagram.

A priori, the position of the band edges at cathodic sites is relatively easy to predict, because it is given by the Schottky electrode limit.[17] The Si/Pt contact acts most likely as a nanosized Schottky contact, which implies that the Fermi level of the platinum cluster is similar to that of the Pt(II) solution ($E_{F,Pt} = 0.4$ V; see Figure 6 and Table 1). This locally fixes the position of the CB of the silicon under the Pt nuclei at $E_{C,Pt} = -0.35$ V and the VB edge at $E_{V,Pt} = +0.75$ V by accounting for the measured Schottky barrier $\Phi_{B,n} = 0.75$ eV (*n*-type Si/Pt). One deduces the value of $\Phi_{B,p}$ to be 0.35 eV (*p*-type Si/Pt). At the anodic sites, and in initial stages, we use the energy diagram measured in the *blank solution* to account for the situation prior to deposition. For *n*-type silicon: $E_{C,Si} = -0.75$ V and $E_{V,Si} = +0.35$ V. For *p*-type silicon: $E_{C,Si} = -0.55$ V and $E_{V,Si} = +0.55$ V. However, the electrode potential is given by the Fermi energy measured in the Pt(II) solution (see Table 1), when the steady state is reached ($E_{F,n} = -0.1$ V and $E_{F,p} = 0$ V).

4.3.1. n-type Silicon Electrode. The following scenario may be proposed. In the initial stages, platinum nucleates on the silicon surface by means of a hole injection process, because the bands are suitably located (Table 1). The top portion of Figure 10 presents the *theoretical* diagrams for the bare (left) and platinum-covered (right) parts of the surface. They were built using the previously described position of bands and using the *final* values (−0.1 V) of the OCP. For *n*-type silicon, $E_{F,n} = -0.1$ V corresponds to a band bending of +0.4 V at the naked silicon surface (between Pt nuclei). At the cathodic sites (Pt/Si contacts), the theoretical band bending should be close to 0 V. This situation is unrealistic, because the associated thermionic emission of electrons from the CB into the Pt nuclei

would be exceedingly large under steady-state conditions and could not be compensated electrochemically.

The magnitude of the anodic current on the naked surface is ca. 100 μA/cm^2. On the other end, the direct current is given by $j_{Pt,Si} = j_0 \exp[eU_S/(nkT)]$ for the *n*-type Si/Pt contact, where U_S is the diode bias (equal to $E_{F,Pt} - U$), *n* is the ideality factor, and $j_0 = A^*T^2 \exp[-q\Phi_B/(kT)] \approx 0.2\ \mu$A/cm^2, with $\Phi_B = 0.75$ eV and $A^* = 12$ A K^{-2} (from ref 17). Assuming that the contact surface between the Pt nuclei and the silicon represents only 1% in the initial stages of deposition, U_S must be $\sim$0.18 V to make $j_{Pt,Si} = j_{inj}$. This implies a local upward shift of the Si band edges, because of the fixed distance $E_{F,Pt} - E_{C,Pt} = \Phi_{B,n} = 0.75$ eV. The shift amounts to ca. -0.19 V. The previously given estimate assumed an ideality factor of $n = 1$. A greater value of *n* would reduce the shift. By construction, the aforementioned shift is also equal to the overpotential developed between the Pt nuclei and the Pt(II) solution. The Pt nuclei are therefore cathodically polarized by ca. 180 mV. Platinum may therefore be deposited on existing Pt clusters in a standard cathodic process (Figure 10, bottom). The previously described situation is approximately valid for the steady-state deposition. With 10% of contact surface, the band edges should increase by 60 mV and amounts to 240 mV, so as to increase the band bending and keep the conditions of current compensation. This does not change the conclusions. The exact magnitude of this overpotential depends on the effective contact surface between the silicon and the platinum, which might be smaller than the diameter of nuclei observed by AFM. In any case, the situation is such that the overpotential is large enough to explain that platinum is deposited under mass-transport control in solution. The injected holes (at Pt sites) may be captured by the potential wells arising from the naked surface ($E_{V,Si}$ lies above $E_{V,Si-Pt}$), where they remain confined to the surface region and lead to silicon dissolution.

In the very initial stages of the deposition, the surface contact may be much smaller than 1%. For a coverage of 10^{-4}, the shift of the band edges would be only 120 mV, which, as expected, sets the positions of the band edges closer to that of the anodic sites on the silicon surface. This favors homogeneous dissolution of the substrate and explains the induction time noticed before observing any metal nuclei. Upon deposition, the overpotential on the Pt nuclei increases, which favors platinum-on-platinum deposition. Therefore, the growth is progressive, in accordance with the SEM observations (Figure 1).

4.3.2. p-type Silicon Electrode. The theoretical diagrams are given at the top of Figure 11. The band bending is -0.5 V at the *p*-type Si/Pt nanocontacts and -0.30 V at the bare surface (recall that the negative sign means an upward band curvature). At the *p*-type Si/Pt contact, the current is again given by $j = A^*T^2 \exp[-q\Phi_B/(kT)] \exp[qU_S/(kT)]$. With $\Phi_{B,p} = 0.4$ eV and $A^* = 12$ A cm^{-2} K,[17] the current density is $\sim$0.2 A/cm^2 in *reverse* bias. In contrast to the case of *n*-type silicon, a balance $j_{inj} = j = 100\ \mu$A/cm^2 is not possible as soon as the coverage exceeds 10^{-5}! This means that the value of $\Phi_{B,p}$ is wrong. To explain these observations, an *apparent* $\Phi_{B,p}$ value of $\sim$0.7 eV is necessary, as in the case of *n*-type silicon. We are inclined to think that the hydrogenation of the subsurface region is responsible for such an increase of the *p*-type Si/Pt barrier height. The compensation of acceptors modifies the profile of bands under the surface, as sketched in Figure 11 (bottom, dotted lines) in a way similar to that searched with the thin layer of *opposite* doping implanted at metal-semiconductor solar cells.[15] This technique is used to increase the initial barrier. By

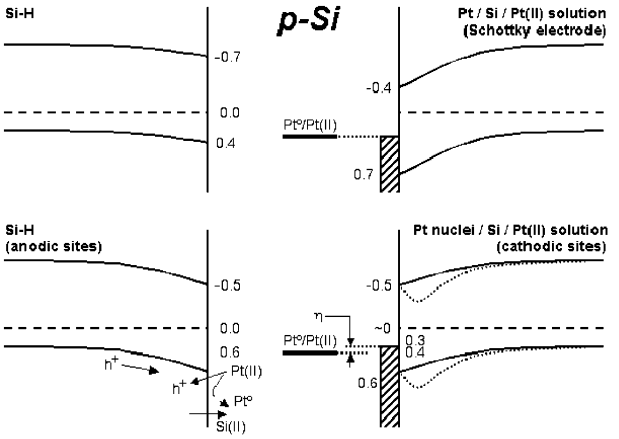

Figure 11. (Top) Theoretical band diagram for the bare and platinum-covered *p*-type silicon surface (see text for the construction). (Bottom) Modified band diagrams. Note the upward shift of the band edges on the cathodic sites. The anodic sites remain unchanged.

selecting the appropriate parameters of the implanted layer (doping density and thickness), the barrier may reach the band-gap value. The near compensation of the subsurface region (over δ, Table 2) and the overcompensation (n^+ layer) of the surface by protons located nearer to the interface (over a few tens of nanometers[30,32]) make this assumption realistic. The effect of hydrogenation may be neglected with *n*-type silicon, because it leads to an overdoped (n^+) sublayer (Table 2), which makes the effective and theoretical barriers very close (the layer may be tunneled by electrons).

To understand the role of hydrogen with *p*-type silicon further, it is worth comparing the deposition of platinum with that of nickel reported earlier.[12] Nickel deposits autocatalytically on silicon from fluoride solutions of pH 8, because the Ni/Ni^{2+} level lies within the silicon band gap. As expected in that case, deposition is accompanied by visible H_2 evolution and no PS formation, whereas at low pH, neither hydrogen nor nickel deposition is observed. It is likely that the higher affinity of nickel to the adsorption of hydrogen and chemical formation of H_2 further precludes hydrogen incorporation into silicon during deposition.

5. Conclusions

An electrochemical study of the open-circuit deposition of platinum on silicon from fluoride solutions has been presented. The main features of the process can be explained using the mixed potential theory, in which the electrode potential is defined by two simultaneous reactions at the electrode surface: platinum reduction and deposition (cathodic reaction), and silicon oxidation and dissolution (anodic reaction). The electron energy diagrams at the anodic and cathodic sites are useful tools to investigate the details of the half-cell reactions. In the steady-state, platinum deposition proceeds by hole injection into the Si valence band through the platinum/silicon interface. At the anodic sites, hydrogen is incorporated into the substrate during the silicon dissolution process. The coupling between the anodic and cathodic half-cell reactions is more complex than the charge exchange through the substrate: hydrogen reoxidation at the Pt nuclei may assist H^+ incorporation into the silicon, and energy-band warping at the anodic regions strongly affect the morphologic distribution of the reacting sites.

Appendix

Considering that a hydrogen-permeated layer has formed between the porous silicon (PS) layer and the silicon substrate,

the calculation of the interface capacitance yields an expression for the apparent flatband (FB) shift as a function of δ (the subsurface thickness), N_S (the thickness and effective doping of the H layer), $N_{A,D}$ (the Si bulk doping), D_H (the diffusion coefficient of hydrogen into the substrate), and R (the etching rate).[16] The time evolution of the apparent FB shift can thus be fitted as a second-order polynomial:

$$\sqrt{\Delta U_{FB}} = A_0 + A_1\sqrt{t} + A_2 t \tag{A1}$$

where A_0 should be almost zero. A_1 and A_2 yield the unknown diffusion coefficient D_H and the relative doping of the layer ($\alpha N_S/N_A$):

$$D_H = \left(\frac{RA_1}{A_2}\right)^2 \tag{A2}$$

$$\frac{\alpha N_S}{N_{A,D}} = \frac{2\epsilon\epsilon_0}{eN_{A,D}}\left(\frac{A_2}{R}\right)^2 - 1 \tag{A3}$$

The etch rate R is a parameter that results directly from the anodic current passed during PS formation, taking into account that a value of 2.66 μA/cm^2 corresponds to an etching rate of 0.1 nm/min for a reaction valency of 2:

$$R = j_{corr}\left(\frac{0.1\ \text{nm min}^{-1}}{2.66\ \mu\text{A cm}^{-2}}\right) \tag{A4}$$

Acknowledgment. The SEM and AFM observations were realized at the Serveis Cientificotècnics (Universitat de Barcelona). P.G. acknowledges fellowship (No. 1999-BEAI-200457) of the DGR (Generalitat de Catalunya) during a visit to the Laboratoire de Physique des Liquides et Electrochimie (CNRS, France). This work was supported by the CICYT (DPI 2000-0703-C-03).

References and Notes

(1) Gorostiza, P. Metal Deposition on Silicon from Fluoride Solutions, Ph.D. Thesis, Universitat de Barcelona, Spain, **2000**. (Manuscript available at http://www.qf.ub.es/a2/a2b/publications.html.)

(2) Dennig, C. Etching and Electrochemical Deposition on Silicon. Application to the Revealing of Junctions, Ph.D. Thesis, Université Paris VI, France, **1991**.

(3) *Wacker's Atlas for the Characterization of Defects in Silicon*, Wacker-Chemitronic GmbH: Burghausen, Germany.

(4) Gorostiza, P.; Servat, J.; Sanz, F.; Morante, J. R. In *Defect Recognition and Image Processing in Semiconductors*; Mickelson, A. R., Ed.; Institute of Physics Publishing Ltd.: Bristol, U.K., **1996**; Vol. 149, p 293.

(5) Teerlinck, I.; Gomes, W. P.; Strubbe, K.; Mertens, P. W.; Heyns, M. M. *1999 ECS Meeting Abstracts*; Electrochemical Society: Pennington, NJ, 1999; Vol. MA 99-1, p 279.

(6) Chyan, O. M. R.; Chen, J. J.; Chien, H. Y.; Wu, J. J.; Liu, M.; Sees, J. A.; Hall, L. H. *J. Electrochem. Soc.* **1996**, *143*, L235.

(7) Reddy, A. J.; Michel, J.; Parekh, B.; Shyu, J.-H.; Kimerling, L. C. *J. Electrochem. Soc.* **2000**, *147*, 2337.

(8) Gorostiza, P.; Diaz, R.; Kulandainathan, M. A.; Sanz, F.; Morante, J. R. *J. Electroanal. Chem.* **1999**, *469*, 48.

(9) Oskam, G.; Long, J. G.; Nikolova, M.; Searson, P. C. *Mater. Res. Soc. Symp. Proc.* **1997**, *451*, 257.

(10) Oskam, G.; Searson, P. C. *J. Phys. D: Appl. Phys.* **1998**, *31*, 1927.

(11) Srinivasan, R.; Suni, I. I. *J. Electrochem. Soc.* **1999**, *146*, 570.

(12) Gorostiza, P.; Diaz, R.; Sanz, F.; Allongue, P.; Morante, J. R. *J. Electrochem. Soc.* **2000**, *147*, 1026.

(13) Gorostiza, P.; Diaz, R.; Servat, J.; Sanz, F.; Morante, J. R. *J. Electrochem. Soc.* **1997**, *144*, 909.

(14) Gorostiza, P.; Diaz, R.; Sanz, F.; Morante, J. R. *J. Electrochem. Soc.* **1997**, *144*, 4119.

(15) Sze, S. M. *Physics of Semiconductor Devices*, 2nd ed.; John Wiley & Sons: New York, 1981.

(16) Allongue, P.; de Villeneuve, C. H.; Pinsard, L.; Bernard, M. C. *Appl. Phys. Lett.* **1995**, *67*, 941.

(17) Allongue, P. In *Modern Aspects of Electrochemistry*; Conway, B. E., Bockris, J. O'M., White, R. E., Eds.; Plenum Press: New York, 1992, Vol. 23.

(18) Allongue, P.; de Villeneuve, C. H.; Pinsard, L.; Bernard, M. C. Unpublished results.

(19) Allongue, P.; Costa-Kieling, V.; Gerischer, H. *J. Electrochem. Soc.* **1993**, *140*, 1009.

(20) Allongue, P.; Costa-Kieling, V.; Gerischer, H. *J. Electrochem. Soc.* **1993**, *140*, 1018.

(21) Allongue, P.; Kieling, V.; Gerischer, H. *Electrochim. Acta* **1995**, *40*, 1353.

(22) Roche, J. R.; Ramonda, M.; Thibaudau, F.; Dumas, P.; Mathiez, P.; Salvan, F.; Allongue, P. *Microsc. Microanal. Microstruct.* **1994**, *5*, 291.

(23) Notten, P. H. L. Electrochemical Study of the Etching of III−V Semiconductors, Ph.D. Thesis, Technische Universiteit Eindhoven, The Netherlands, **1989**.

(24) Gerischer, H.; Lübke, M. *Ber. Bunsen−Ges. Phys. Chem.* **1987**, *91*, 394.

(25) Gerischer, H.; Allongue, P.; Costa-Kieling, V. *Ber. Bunsen−Ges. Phys. Chem.* **1993**, *97*, 753.

(26) Canham, L. T. *Appl. Phys. Lett.* **1990**, *57*, 1046.

(27) Stumper, J.; Peter, L. M. *J. Electroanal. Chem.* **1991**, *309*, 325.

(28) Smith, R. L.; Collins, S. D. *J. Appl. Phys.* **1992**, *71*, R1.

(29) Fathauer, R. W.; George, T.; Ksendzov, A.; Vasquez, R. P. *Appl. Phys. Lett.* **1992**, *60*, 995.

(30) Pearton, S. J.; Corbett, J. W.; Shi, T. S. *Appl. Phys. A* **1987**, *43*, 153.

(31) Rizk, R.; de Mierry, P.; Ballutaud, D.; Aucouturier, M.; Mathiot, D. *Phys. Rev. B* **1991**, *44*, 6141 and references therein.

(32) Allongue, P.; de Villeneuve, C. H.; Bernard, M. C.; Péou, J. E.; Boutry-Forveille, A.; Lévy-Clement, C. *Thin Solid Films* **1997**, *297*, 1.